The Egyptian Journal of Remote Sensing and Space Sciences xxx (xxxx) xxx

HOSTED BY

ELSEVIER

Contents lists available at ScienceDirect

The Egyptian Journal of Remote Sensing and Space Sciences

journal homepage: www.sciencedirect.com

Research Paper

Trends in land surface temperature and its drivers over the High Mountain Asia

Seema Rani [a,*], Suraj Mal [b]

[a] Department of Geography, Institute of Science, Banaras Hindu University, Varanasi, Uttar Pradesh, India
[b] Department of Geography, Shaheed Bhagat Singh College, University of Delhi, New Delhi, India

ARTICLE INFO

Article history:
Received 3 October 2021
Revised 27 March 2022
Accepted 26 April 2022
Available online xxxx

Keywords:
Land surface temperature
Elevation-dependent warming
High Mountain Asia

ABSTRACT

The present study estimates spatial and temporal (seasonal/annual) trends in daytime land surface temperature (LST) and its drivers (elevation, cloud fraction (CF), atmospheric water vapor (AWV), normalized difference vegetation index (NDVI), and snow cover area (SCA)) over the High Mountain Asia (HMA) during 2001–2019 using MODIS remote sensing data. The findings of the study showed mixed trends in LST in the region with intra-regional variations. Overall, the warming in the region is attributed to increasing AWV and NDVI and declining CF and SCA. The study also found evidence of elevation-dependent warming (EDW) (4500–5500 m AMSL) in some regions. However, the same conclusion cannot be drawn in all the sub-regions of HMA, suggesting the need to explore the effects of additional natural and anthropogenic factors on LST with fine resolution data to improve the understanding of its spatio-temporal dynamics.

1. Introduction

Land surface temperature (LST) is one of the key dynamic surface conditions that help in understanding the earth surface energy balance and estimating some atmospheric variables (Hereher, 2019; Prakash et al., 2019; Rao et al., 2019; Singh et al., 2020) in the mountain regions, where limited station based climate variables are available (Kuenzer and Dech, 2013). The study of LST dynamics is critical for a better understanding of its impact on regional climates (Jaber and Abu-Allaban, 2020; Mal et al., 2021), surface energy balance (Khandelwal et al., 2018), surface/groundwater hydrology (Zhao et al., 2020a), vegetation phenology (Li et al., 2021), human health (Avashia et al., 2021), temperature hot spots (Mildrexler et al., 2011) and characterizing land use/land cover (LULC) (Mildrexler et al., 2018). The mean temperature was 1.2 ± 0.1 °C (at global scale) and 1.39 °C (in Asia) for 2020 that is above the 1850–1900 baseline data (WMO, 2020a,b). Concerning global climate change and its significance, various research examined the spatiotemporal variations in LST using station-based measurements and dynamical climate models (Sharifnezhadazizi et al., 2019; Prakash and Norouzi, 2020). Global LST has been rising during 2001–2017 (Song et al., 2018; Liu et al., 2021). Li et al. (2020) observed significant warming (air temperature) (0.323 °C/decade) in Tianshan Mountains (TSM), Northern Tibetan Plateau (NTP), Southeastern Tibetan Plateau (SETP), Southwestern Tibetan Plateau (SWTP) of the High Mountain Asia (HMA) during 1961–2017. Concerning the HMA, studies have revealed warming in Central Tien Shan Mountains (Sun et al., 2015), Kashmir Himalaya (Romshoo, Rafiq and Rashid 2018), the central Himalayas (CH) (at the rate of 0.102–0.190 °C/yr during 2000–2017) (Zhao et al., 2019), the Hindu Kush Himalayas (HKH) (Krishnan et al., 2020), Qinghai-Tibetan Plateau (Zou et al., 2020; Zhao et al., 2020b) and TP (Yang et al., 2021). During the period 2003–2019, Song et al. (2021) found a warming trend in daytime LST in the middle of the TP, as well as the middle and western areas of Inner Mongolia. However, warming patterns in LST are not consistent over the HMA, which needs further investigation. A report also predicted an increase in annual mean LST in the Himalayas of around 5.2 °C by the end of the twenty-first century (Krishnan et al., 2020). According to the Intergovernmental Panel on Climate Change (IPCC, 2018), high mountain regions would be the most affected by future global warming of 1.5 °C. As a result, intra-regional thorough research of variations in LST in the HMA is required, which, to the best of our understanding, is currently lacking.

Several factors influence LST changes, including atmospheric (e.g., insolation, air temperature, angle of incidence of solar radiation, cloud cover) and surface properties (e.g., surface roughness, vegetation cover, emissivity, albedo, the heat capacity of surface

* Corresponding author.
E-mail addresses: seemarani@bhu.ac.in (S. Rani), suraj.mal@sbs.du.ac.in (S. Mal).

https://doi.org/10.1016/j.ejrs.2022.04.005
1110-9823/

soil layers, soil moisture, and local topography) (Song et al., 2018; Khandelwal et al., 2018; Khandan et al., 2018; Thiebault and Young, 2020; Zou et al., 2020; Song et al., 2021; Liu et al., 2021). However, even though it offers substantial positive feedback for global warming as well as other greenhouse gases (e.g., methane), the influence of atmospheric water vapour (AWV) on variations in LST has received little attention (Held and Soden, 2000). These factors point to the difficulty in comprehending the spatiotemporal process of LST. There is a scarcity of in-depth studies on these factors in the HMA. The reported changes in LST might have serious consequences on an area's physical system, particularly in the mountains (such as surface energy balance, glaciers melting, decreasing perennial snow cover and permafrost, and decreased water availability) (Hock et al., 2019; Mildrexler et al., 2018; World Meteorological Organization (WMO), 2020a). As a result, this would have an impact on the livelihoods of millions of people in the surrounding region. Thus, its examination is required for appropriate planning and management of the region's natural resources.

Several studies used satellite-based LST data because of its extensive spatial coverage, high resolution, and long-term availability (Sharifnezhadazizi et al., 2019; Zhao et al., 2019; Prakash and Norouzi, 2020). To the best of our knowledge, the HMA has not been exposed to extensive regional LST trend studies and its drivers, particularly AWV. Thus, the present paper is attempted i) to investigate the seasonal/annual trends in LST using remote sensing monthly data from 2001 to 2019, ii) to assess the main drivers of LST trends, including elevation, AWV, cloud fraction (CF), normalized difference vegetation index (NDVI), and snow cover area (SCA). This study would enhance the understanding of dynamics in LST and its drivers over the HMA.

2. Study area

The present study was conducted in the HMA, which is the world's largest glacierized region outside of the polar regions, also popularly known as "The Third Pole" (Bolch et al., 2012, 2019). It is a high-altitude area of Asia that encompasses East, South East, Central, and South Asia (Fig. 1). It includes Hindukush-Karakorum-Himalayan mountain ranges, Kunlun, Tien Shan, Altai and Pamir mountain ranges. This region spans China, Afghanistan, Nepal, India, Pakistan, Bhutan, Kazakhstan, Uzbekistan, Kyrgyzstan, and Tajikistan countries. Bolch et al. (2019), has subdivided the HMA into 22 regions (Fig. 1). This region has undulating terrain ranging between ~500 m above mean sea level (AMSL) in the southern Himalayan rim and 8850 m AMSL (Everest peak), steep hillslopes, a cold climate, and spatial inaccessibility (). The HMA supports 10 large rivers in the region, including the Indus, Ganges, and Brahmaputra rivers. About 10% of the world's population lived in high mountain areas in 2010 (Jones and O'Neill, 2016). Considering the socioeconomic scenarios, its population is anticipated to expand to 736–844 million by 2050 (Gao, 2019).

3. Materials and method

The present study used the Moderate Resolution Imaging Spectroradiometer (MODIS) LST, AWV, CF, NDVI, and SCA monthly data (Jan 2001–Dec 2019) obtained from the Earthdata (https://earthdata.nasa.gov/) (Table 1 and Fig. 2). The MODIS LST products have values of clear sky to reduce the cloud cover impact, which is the main constraint in its application (Sun et al., 2015). Fewer clear sky days (e.g. <10 days) in a monthly LST product increase its uncertainty depending on the location of a region. However, the random cloud-cover occurrence has a lesser influence on monthly LST, which enhanced its spatio-temporal integrity and consistency as compared to daily and 8 days' composite data (Zhao et al., 2020b). MODIS Terra (MOD11C3 ver 6 at 0.05° × 0.05°) monthly clear sky daytime LST data (Jan 2001 - Dec 2019) are used in the present study (https://earthdata.nasa.gov/eosdis/daacs/lpdaac) (Earthdata Search, 2019; Wan, 2015; Wan, 2013) because its accessibility and consistency increase with spatial and temporal aggregation resulting in fewer data gaps, compared to night-time LST. Furthermore, the accuracy of the daytime LST ver. 6 products has improved over the ver. 5 product when compared to nighttime LST (Lu et al., 2018) due to significant improvements in retrieval methods (Duan et al., 2019). MODIS MOD08 M3 AWV and CF (1° × 1°) L3 daytime data have been used to investigate their relationship with LST across the region (Platnick et al., 2015). MODIS MOD13C2 NDVI (0.05° × 0.05°) L3 data are cloud-free spatial composites that were used in this study to determine the region's vegetation characteristics and their influence on LST (Didan, 2015).

MODIS MOD10CM (Terra) SCA (L3 global at 0.05° × 0.05°) was used in the current study to estimate SCA since it is a key variable in high elevation areas of the HMA that has a significant impact on LST (Hall and Riggs, 2015). Overall, when compared to other sources of global or regional snow cover data, the MOD10CM appears to be a fair depiction of mean monthly SCA (Riggs et al., 2019) and is extensively used for examining changes in SCA throughout the Himalayas (Shafiq et al., 2019). The digital elevation model (DEM) (250 m) of the Shuttle Radar Topography Mission v4.1 (SRTM obtained from https://earthdata.nasa.gov/) was used to comprehend the topographic information (500 m elevation bands/zones) (Fig. 1) and its interaction with the LST of the study area (Jarvis et al., 2008).

All the MODIS data used in the study has been resampled to 0.05° × 0.05° using the nearest neighbour approach and subsets of the study region were generated (Fig. 2). The seasonal and annual series were then generated from the monthly data for all parameters used in the study area. The Theil Sen's Slope estimator (Theil, 1950; Sen, 1968) was used to estimate seasonal/annual trends (2001–2019), and its significance was assessed using the Mann-Kendall test (at 0.10 sig. level) (Kendall, 1975; Neeti and Eastman, 2011). The estimated significant trends magnitude (LST, NDVI, SCA) are also obtained across 12 elevation zones. The spatial correlations of LST with other variables (elevation, CF, AWV, NDVI, and SCA) were estimated using Pearson Product Moment correlation (tested at 0.01 significance level) in System for Automated Geoscientific Analyses (SAGA) (Conrad et al., 2015). The present study used the traditional quarters of four seasons: winter (DJF), spring (MAM), summer (JJA), and autumn (SON).

4. Results

4.1. Spatial distribution of mean LST

The mean annual daytime LST is estimated as 11.5 °C (σ: 6.9 °C) for the entire HMA during 2001–2019. The corresponding LST is observed as lowest in the winter season (mean −0.86 °C, σ: 8.6 °C) and highest in the summers (mean: 20.9 °C, σ: 8.2 °C). The estimated LST is slightly low during spring (mean 13.8 °C, σ: 8.1 °C) and autumn (mean: 12 °C, σ: 6.6 °C) (Fig. S1). Among all the regions of the HMA, the ETS region observed pronounced seasonal variations in daytime LST from a maximum in summer (29 °C) to a minimum in winter (−8 °C), followed by the DA (summer: 25 °C and winter: −11 °C) and WP regions (summer: 22 °C and winter: −13 °C) (Fig. S1). During the study period, EH had the lowest range of mean LST, followed by N and HS. Among the 22 HMA regions, four regions (WP, K, DA, and CTS) have LSTs <−10 °C during the winter, while only one (AS) has LSTs >30 °C during the summer (Fig. S1). Among all HMA regions, K is the cold-

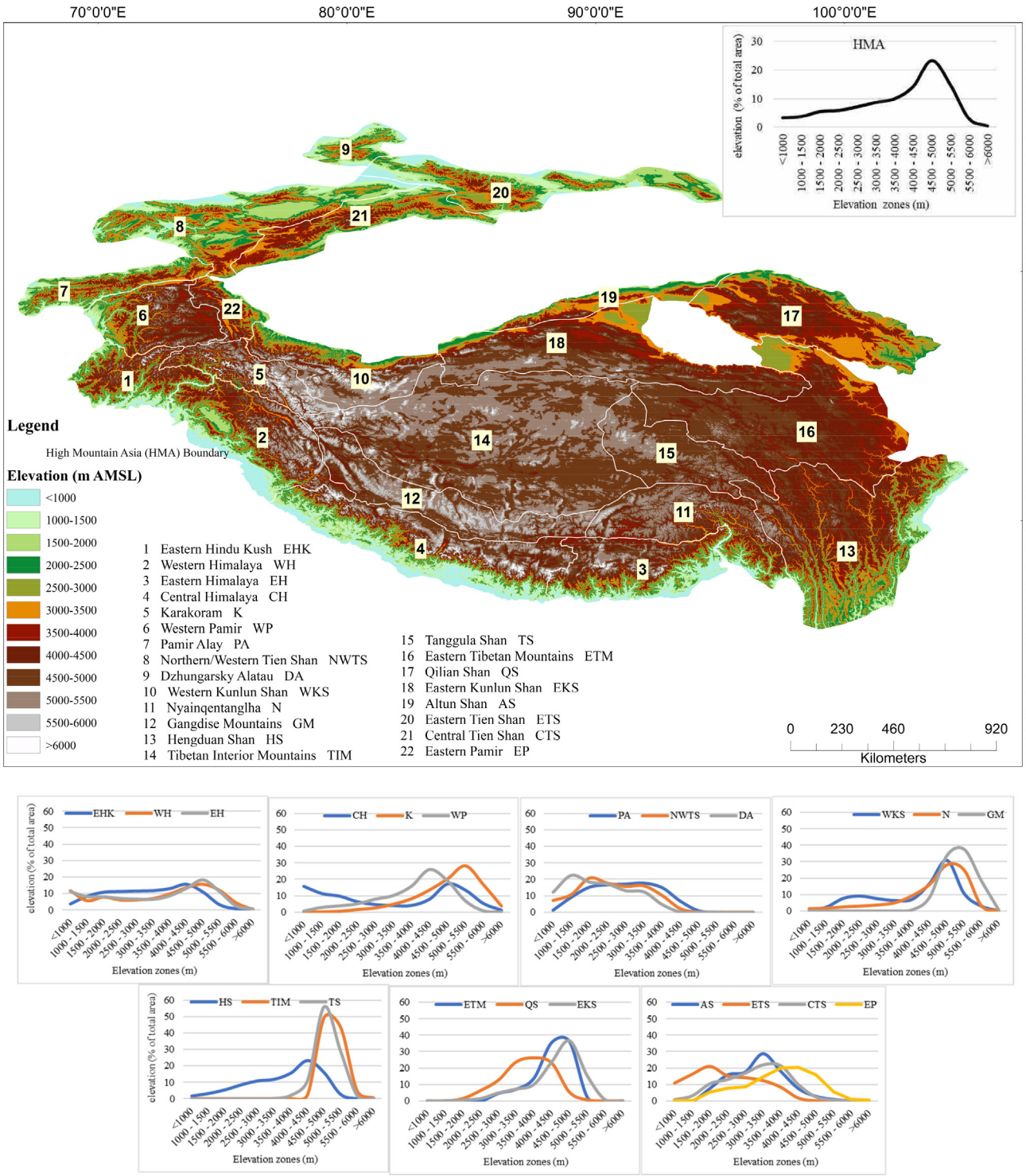

Fig. 1. Location and extent of the HMA. The background shows the distribution of elevation over the HMA based on SRTM 250 m. Graphs show the distribution of elevation (%) in different mountain regions of the HMA. The HMA is divided into 22 regions based on Bolch et al. (2019).

Table 1
Description of datasets used in this study.

Datasets	Drivers	Version	Layer name	Unit	Spatial resolution	Temporal resolution
MOD11C3	LST	ver 6	LST_Day_CMG	Kelvin	0.05 deg	monthly
MOD08_M3	AWV	ver 6.1	Atmospheric_Water_Vapor	cm	1 deg	monthly
MOD08_M3	CF	ver 6.1	Cloud_Fraction_Day	none	1 deg	monthly
MOD13C2	NDVI	ver 6	CMG 0.05 Deg Monthly NDVI	none	0.05 deg	monthly
MOD10CM	SCA	ver 6.1	Snow_Cover_Monthly_CMG	%	0.05 deg	monthly
Shuttle Radar Topography Mission (SRTM)	Elevation	v4.1	–	meter	250 m	–

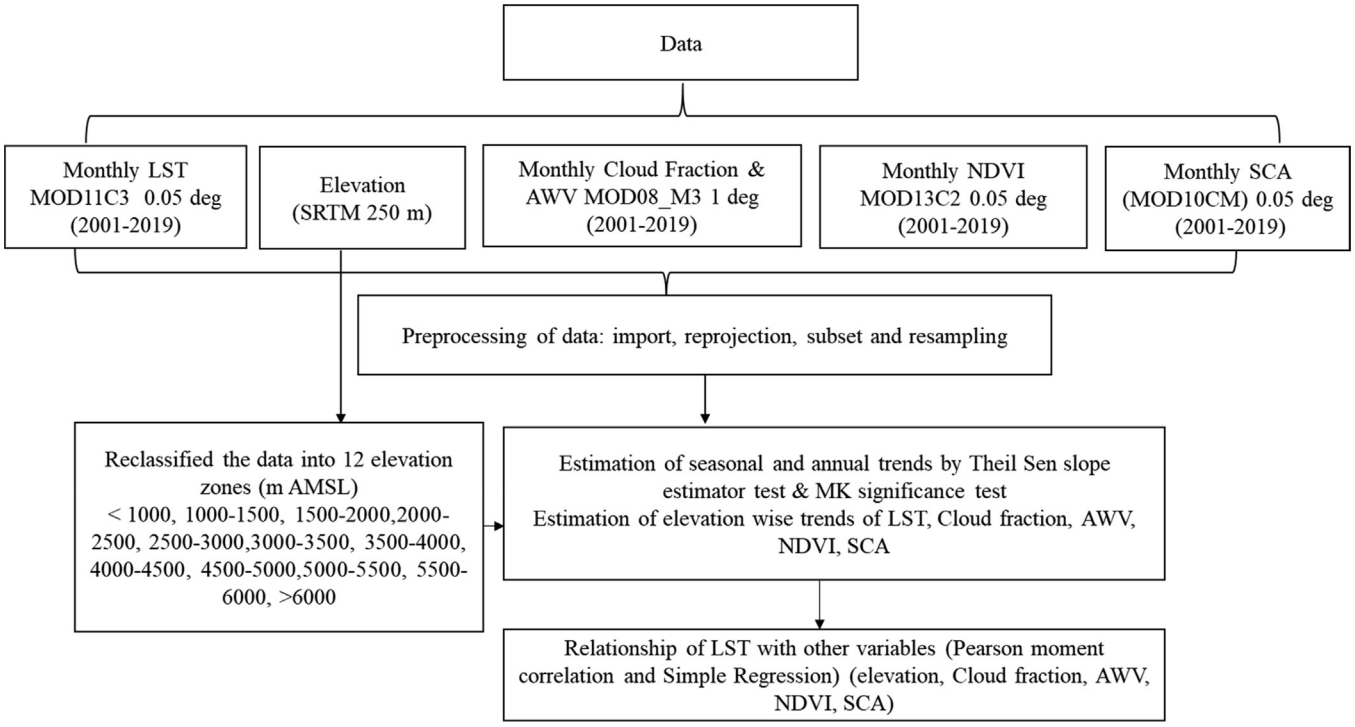

Fig. 2. Data and methodological flow of the present study.

est and AS is the warmest, owing to the geographical and elevation distribution, atmospheric and surface characteristics (Dimri, 2021).

4.2. Elevation wise mean LST

The elevation has a considerable impact on the spatial distribution of mean daytime LST (Peng et al., 2017). A significant inverse relationship between mean LST and elevation across all seasons is observed (right-panel of Fig. S1 and Table 2), which is consistent with earlier studies (Khandelwal et al., 2018; Peng et al., 2020; Mal et al., 2021; Yang et al., 2021). Summer has the highest daytime LST lapse rate (3.4 °C/km), followed by spring (2.7 °C/km), autumn (2.6 °C/km), and winter (1.6 °C/km) (Fig. S1). During the winter, the land surface in the mountains cools significantly, decreasing the LST range and, as a result, the lapse rate. The highest temperature lapse rate in the HMA during the summer might be due to latent heating at higher elevations (Kattel et al., 2013). Furthermore, regional differences in temperature lapse rates in the HMA are caused by a variety of geographical, atmospheric (temperature inversion) and topographical conditions (Li et al., 2013). The mean annual daytime LST is 2.6 °C/km in the HMA (Fig. S1). In the current study, the estimated temperature lapse rates at seasonal and annual scales are lower than the air temperature lapse rates as observed (−6.1 to −4.3 °C/km) in the CH by Kattel et al. (2013), which might be related to the complex elevation conditions of the CH. Another reason for the lower MODIS daytime LST lapse rate as observed in the study might be that daytime LST is less representative of air temperature lapse rate, as compared to the MODIS nighttime LST lapse rates (Zhang et al., 2018b).

4.3. Trends in mean LST

Seasonal mean daytime LST has shown a significant rising trend (at 0.10) at the average rates of 0.04 °C/yr, 0.03 °C/yr, and 0.04 °C/yr over HMA during winter, spring, and summer, respectively. However, a declining LST trend (−0.07 °C/yr) is observed during autumn (Fig. 3a). The study region likewise shows a rising trend in the mean annual LST (0.01 °C/yr) (Fig. 3a). Annual and seasonal mean LST trends are also estimated in different sub mountain regions (Fig. 3b). During the study period, EH, WP, PA, NWTS, DA, N, GM, HS, TIM, TS, and CTS witnessed considerable warming (Fig. 3b). WP and TS observed the highest annual warming rates, whereas certain locations (EHK, WH, WKS, EKS, etc.) have shown cooling trends (Fig. 3b).

There is no consistent spatial pattern of trends in mean LST across different NDVI zones (Fig. 4a). During the study period, mean LST exhibited a substantial declining trend in winter, spring, and autumn in the NDVI zone between 0.50 and 0.75 and a rising

Table 2
Correlation of mean LST with elevation, AWV, CF, NDVI and SCA in the HMA.

Drivers	Mean LST				
	Winter	Spring	Summer	Autumn	Annual
Elevation	−0.242**	−0.459**	−0.562**	−0.538**	−0.509**
AWV	0.470**	0.328**	0.176**	0.408**	0.433**
CF	−0.647**	−0.404**	−0.421**	−0.258**	−0.267**
NDVI	0.699**	0.399**	−0.073**	0.309**	0.364**
SCA	−0.768**	−0.845**	−0.550**	−0.781**	−0.777**

** Significant at 0.01 level (2-tailed).

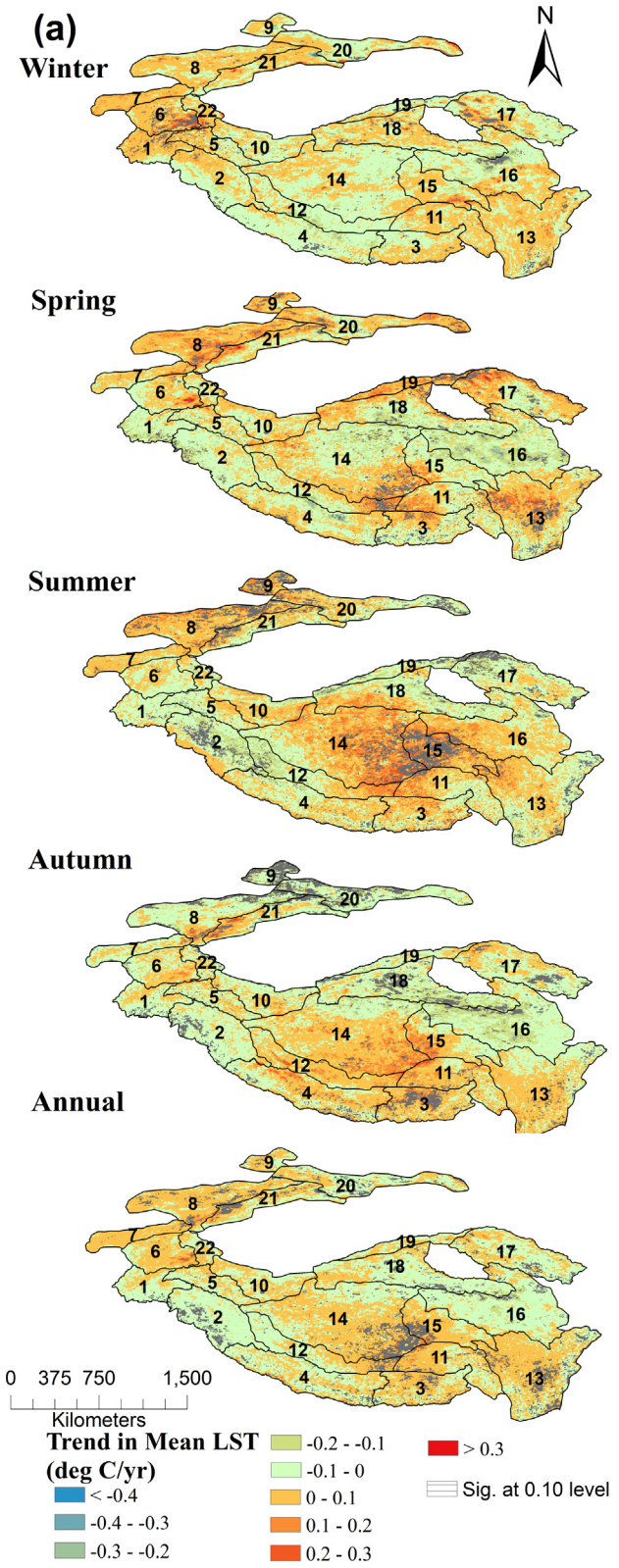

(b)

LST (deg C/yr)

	Winter	Spring	Summer	Autumn	Annual
HMA	0.04	0.03	0.04	-0.07	0.01
EHK	0.13	-0.13	-0.07	-0.10	-0.07
WH	-0.01	-0.15	-0.13	-0.10	-0.08
EH	0.05	0.00	0.07	0.13	0.06
CH	-0.06	0.03	-0.02	0.03	-0.01
K	0.07	-0.04	-0.10	-0.04	-0.05
WP	0.20	0.08	-0.02	-0.13	0.13
PA	0.10	0.15	0.12	-0.04	0.09
NWTS	0.10	0.19	0.13	-0.12	0.07
DA	-0.23	0.17	0.12	-0.16	0.03
WKS	-0.07	-0.17	-0.09	-0.08	-0.10
N	0.05	0.06	0.13	0.09	0.08
GM	-0.10	0.17	-0.14	0.10	0.07
HS	0.03	0.11	-0.02	0.03	0.04
TIM	-0.11	-0.01	0.20	0.05	0.07
TS	0.19	-0.02	0.18	0.03	0.10
ETM	-0.14	-0.16	0.02	-0.20	-0.12
QS	0.16	0.05	-0.16	-0.09	-0.04
EKS	0.02	-0.08	-0.20	-0.18	-0.12
AS	-0.06	0.15	-0.15	-0.05	0.02
ETS	0.04	0.11	-0.04	-0.14	-0.05
CTS	0.05	0.05	0.08	-0.04	0.07
EP	0.19	-0.08	-0.14	-0.09	-0.08

Scale: -0.25, -0.20, -0.15, -0.10, -0.05, 0, 0.05, 0.10, 0.15, 0.20, 0.25

Fig. 3. (a) Spatial distribution of the mean LST trends over the HMA between 2001 and 2019 (b) Region wise mean LST trends between 2001 and 2019 (at 0.10 sig level).

trend in winter and autumn in the NDVI zone between 0.75 and 1. During the summer, the highest increase in mean LST was seen between NDVI values of 0.25 and 0.50 over the HMA. The study found a warming trend in annual mean LST at elevations more than 4500 m (Fig. 4b). Furthermore, there is a noticeable warming trend between 4500 and 6000 m (0.01–0.16 °C/yr) in winter, spring, and summer, confirming the EDW process. In the winter and summer, cooling is also observed at elevations above 6000 m in the HMA (Fig. 4b). However, some mountain regions in the HMA are experiencing warming trends in the different seasons above 6000 m (Fig. 5). Warming trends in elevations more than 6000 m throughout winter (EHK, WH), spring (EHK, EH, CH, K, WP, WKS, HS, TIM),

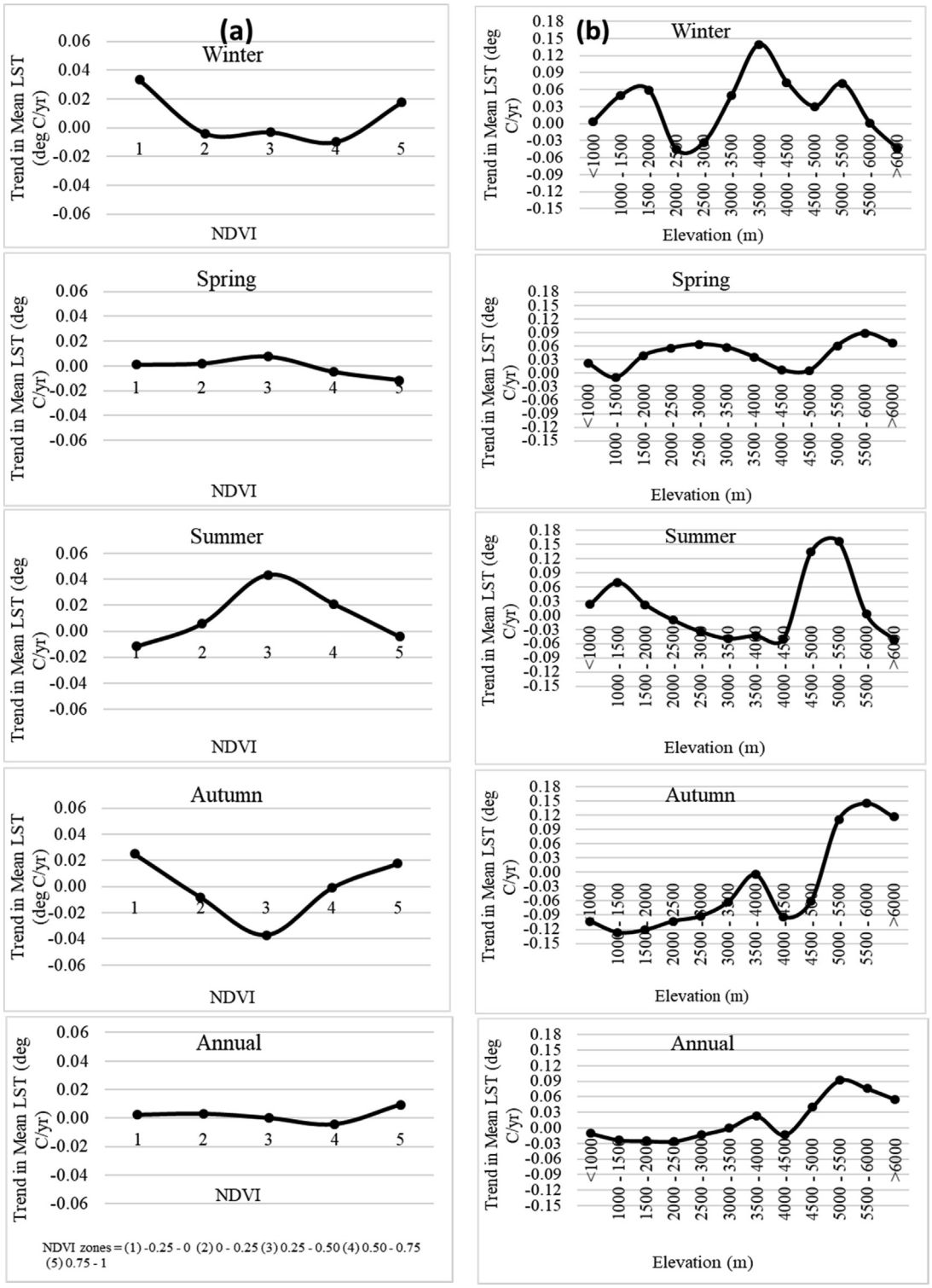

Fig. 4. (a) NDVI zone wise and (b) elevation zone wise mean LST trends over the HMA during 2001–2019. (all the given values are sig. at the 0.10 level).

summer (N, TIM, TS), and autumn (EH, CH, K, N, GM, HS, TIM, TS) are seen. The TIM is experiencing pronounced warming in all the seasons at elevations of more than 6000 m (Fig. 5).

4.4. Key drivers of mean LST changes

4.4.1. Relationship of LST with AWV

AWV reflects and absorbs solar radiation, altering the energy balance directly. It causes a 'positive feedback loop' in the atmosphere, influencing other components, e.g., temperature. Over the HMA, AWV concentrations are highest in summer (1.43 cm) and lowest in autumn (0.73 cm) (Fig. S2). During the study period, the annual AWV in the HMA ranges from 0.31 to 3.8 cm (Fig. S2). A substantial positive relationship between AWV and LST over the HMA in all seasons is seen, resulting in a 'positive feedback loop' in the atmosphere (Table 2 and Fig. S3). Overall, AWV levels indicate an increasing trend over the HMA in all the seasons, except winters where AWV trends remain nearly unchanged

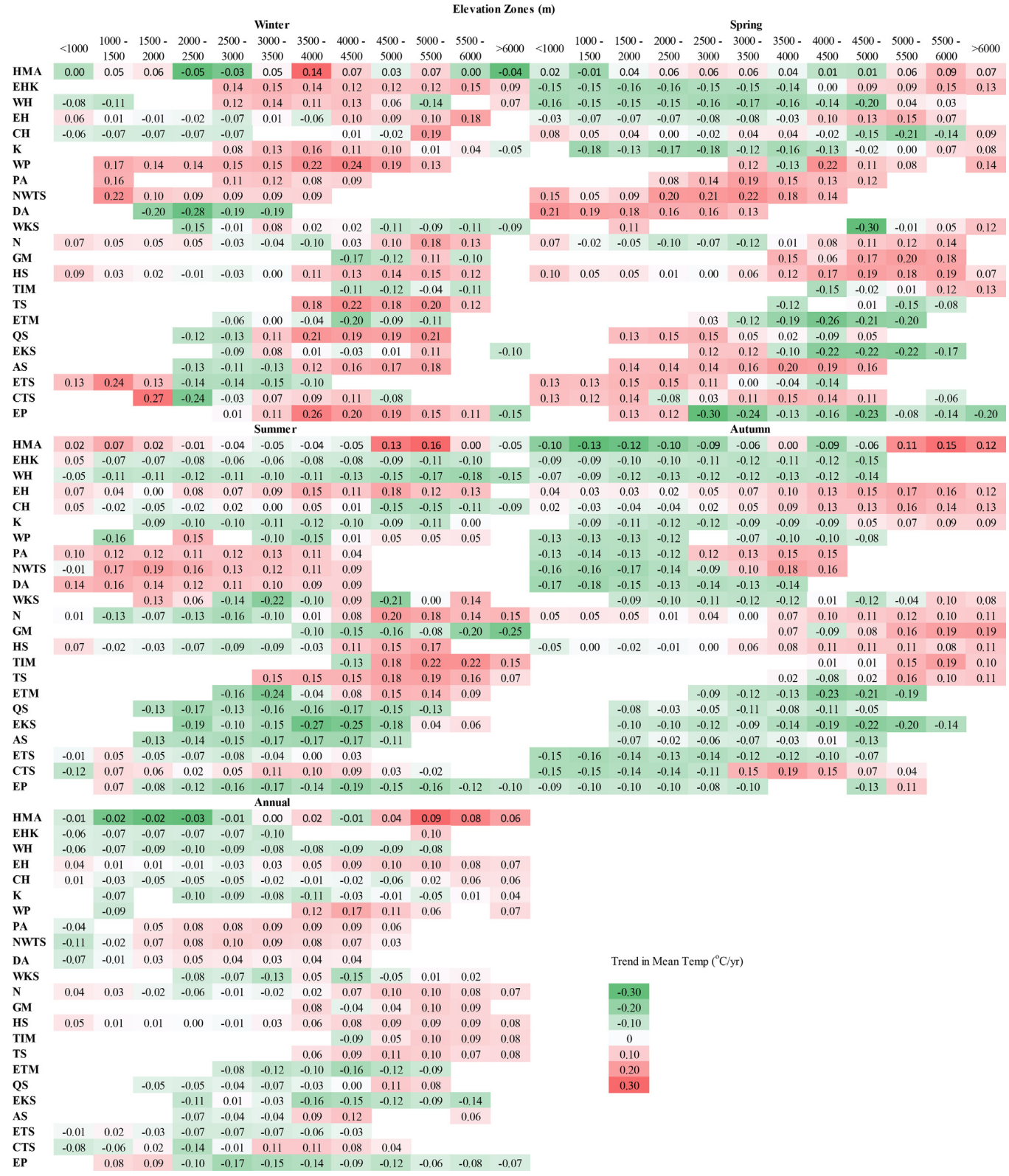

Fig. 5. Region wise mean LST trends (at 0.10 level of Sig.) under different elevation zones over the HMA between 2001 and 2019. Empty boxes in the heat map show no significant trend.

(Figs. S4a and S5a). Summer has the highest rising trend (0.0061–0.0154 cm/yr) in AWV when compared to other seasons. Annual AWV increased at a rate varying from 0.003 cm/yr (WP) to 0.083 cm/yr (CH) over the study period (Fig. S4a and S5a).

4.4.2. Relationship of LST with CF

Cloud cover is another key atmospheric factor that influences the LST conditions. Summer has the highest concentration of CF (56%) over the HMA, followed by winter (55%), spring (54%), and

autumn (43%) (Fig. S2). During the study period, annual CF in the HMA ranged from 29 percent in the TIM to 86 percent in parts of ETM, N, TS, and HS (Fig. S2). The current findings revealed an inverse relationship between the LST and CF (Table 2 and Fig. S3). The present study has demonstrated a substantial decrease in CF across the HMA during winter, whereas the other seasons showed an increase (Fig. S4b and S5b). During winter, there is a decrease in cloud cover (−0.09 - −0.52 percent /yr) over the central regions of the HMA (Figs. S4b and S5b). During the autumn, a strong rising trend (0.24–0.45 percent /yr) was seen in the HMA's south and southeast parts. The same places have experienced a considerable decline in mean daytime LST, which may be ascribed to changes in the local CF conditions (Fig. S1). Except for winter, the EHK and WH have shown a declining trend in CF (0.22 - 0.54 percent/year) (Figs. S4b and S5b). Summer has negligible cloud cover over the HMA from 2001 to 2019. Overall, the research found a substantial negative influence of CF over the mean LST in the HMA in spring and autumn.

4.4.3. Relationship of LST with NDVI

Surface-type conditions such as NDVI have a considerable impact on LST (Tan et al., 2020). The higher NDVI values are mostly concentrated along the southern rim of the Himalayas, HS, and ETM. In the HMA, the mean annual NDVI value is ∼0.22, where the mean NDVI is highest in summer (0.33), followed by autumn (0.25) (Fig. S6). The current research found that LST conditions are positively related to NDVI in all seasons (except summers) in the HMA during the study period (Fig. S1, S6, and S7). Summer has the highest NDVI increase (0.002/yr), followed by autumn (0.0016/yr), spring (0.0015/yr), and winter (0.0012/yr) in the HMA. The annual NDVI trend is estimated as 0.0015/yr (Fig. S8). The region-wise mean NDVI trends (sig. at 0.10) likewise revealed a rising trend in most of the elevation zones (Fig. S9).

4.4.4. Relationship of LST with SCA

SCA is a highly dynamic land surface in the HMA that changes considerably with seasons, with winter (36%) being the highest, followed by spring (28%), autumn (18%), and summer (9%) (Fig. S6). Annual SCA in the HMA ranged from 8 percent (HA) to 59 percent (K) (Fig. S6). LST has a substantial inverse relationship with SCA in all seasons (Table 2 and Fig. S7). SCA decreased at an annual rate of −0.36 percent in winter, −0.08 percent in summer, while increased at an annual rate of 0.22 percent in spring, and with 0.05 percent in autumn (Fig. S8). Annual SCA in the HMA decreased at a mean rate of −0.05 percent/yr (Fig. S8). Elevation has a considerable impact on SCA distribution, hence its trend along elevation is evaluated in the HMA (Jain et al., 2009). Thus, the elevation-wise analysis in SCA demonstrates mixed trends across the region at differing rates (Fig. S10).

5. Discussion

The present study found a considerably increasing trend in LST at the seasonal (excluding autumn) and yearly scales in the HMA between 2001 and 2019, which corroborates with the previous studies in the region (Sun et al., 2015; Romshoo et al., 2018; Zhao et al., 2019; Krishnan et al., 2020; Zou et al., 2020; Zhao et al., 2020b; Song et al., 2021). Zhao et al. (2019) found a rising (0.102 °C/yr) trend in mean annual LST across the CH area from 2000 to 2017. Further, the strength of this fluctuation is often higher in the mountains, as discovered in the current study (Zhao et al., 2019). Pepin et al. (2019) observed an increase in LST at a mean rate of 0.11 °C/decade over the TP (central HMA) from 2002 to 2017. Luintel et al. (2019) detected a shallow warming trend in daytime LST across Nepal, particularly in the foot-hill regions (CH) (2000–2017).

Between 3000 and 3500 m AMSL (which is ∼8% of the HMA), a cooling trend in summer and autumn mean daytime LST is observed in some mountain regions e.g., EHK, WH, CH, K, WP, WKS, N, ETM, QS, EKS, AS, ETS, which could be attributed to increasing SCA and CF. The present study reveals that some regions (e.g. K) are facing cooling trends, which is consistent with the previous study of Zafar et al. (2016) who found that the temperature in the K region has been clearly out of sync with hemisphere temperature patterns for at least the last five centuries. Other studies dealing with glaciers and SCA, which is a direct indicator of climate change, reveal cooling in the K region (Dimri 2021; Bilal et al., 2019). A significant warming trend in yearly mean LST is seen in the elevations ranging from 4500 m to 5500 m, reflecting the EDW process. However, cooling is also recorded in more than 6000 m elevations during the winter and summer. Qin et al. (2009) detected pronounced warming up to 5000 m elevation in TP, however, LST has remained unchanged at higher elevations (>5000 m). Gao et al. (2018) also said that there has been no incidence of EDW over 5000 m in the TP and that it is unlikely to occur in the next decades. During 2002–2017, Pepin et al. (2019) discovered little EDW in the Qilian Mountains. The current findings are consistent with earlier researches, which have shown that the rate of surface warming increases with elevation up to 5000 m (Tan et al., 2020; Li et al., 2020; Mal et al., 2021). EDW has been observed in the HMA (Pepin et al., 2015), which is attributed to a decrease in the SCA. During the period 2000–2017, Zhao et al. (2019) observed that the steep topographic gradient has a substantial influence on the change rate and proved a considerable EDW effect, particularly for the night-time LST. They also noted the declining trend in the daytime LST rate in low elevation regions (<1600 m). However, absolute cooling over 6000 m has been seen, probably as a result of frequent cloud cover.

The study further explores the drivers (AWV, CF, NDVI, and SCA) of LST trends in the HMA. Correlation reveals an insignificant positive relationship between AWV and LST trends over the HMA in all seasons, resulting in a 'positive feedback loop' in the atmosphere (Fig. 6A). This occurs because, at higher temperatures, AWV does not quickly condense and precipitate out of the atmosphere. AWV absorbs the heat released from Earth, preventing it from escaping into space and escalating atmospheric warming, resulting in even more water vapour in the atmosphere, known as a 'positive feedback loop'. The rising AWV trend as observed in the current study is consistent with global and regional research (Lu et al., 2015; Chen and Liu, 2016; Wang et al., 2016; Zhang et al., 2018a; Ho et al., 2018; Yue et al., 2019; Wang and Liu, 2020). Water vapour concentrations rise, amplifying the greenhouse effect and hence the temperature rise (Held and Soden, 2000).

The study revealed an inverse relationship between LST and CF, confirming that CF has a negative effect on LST (Fig. 6B). Clouds regulate the temperature by reflecting parts of the incoming solar energy back into space during the day. Consequently, the incoming solar energy is lowered at the earth's surface, causing the earth to heat up slowly and resulting in lower temperatures. In the HMA, CF increased significantly in all seasons except winter, but there are regional variations. The findings are in agreement with a global trend in cloud cover conditions (Mishra, 2019; Kebiao et al., 2019). The pattern of decreasing cloud cover over TP is consistent with earlier investigations (Lei et al., 2020; Ma et al., 2021). According to Ma et al. (2021), the decreasing trend of CF in the region is due to Rossby wave trains across the Eurasian region and the weakening of the South Asia High. However, other places (PA, WKS, EP, etc.) have exhibited no trend in some seasons in the HMA, necessitating further examination in the future.

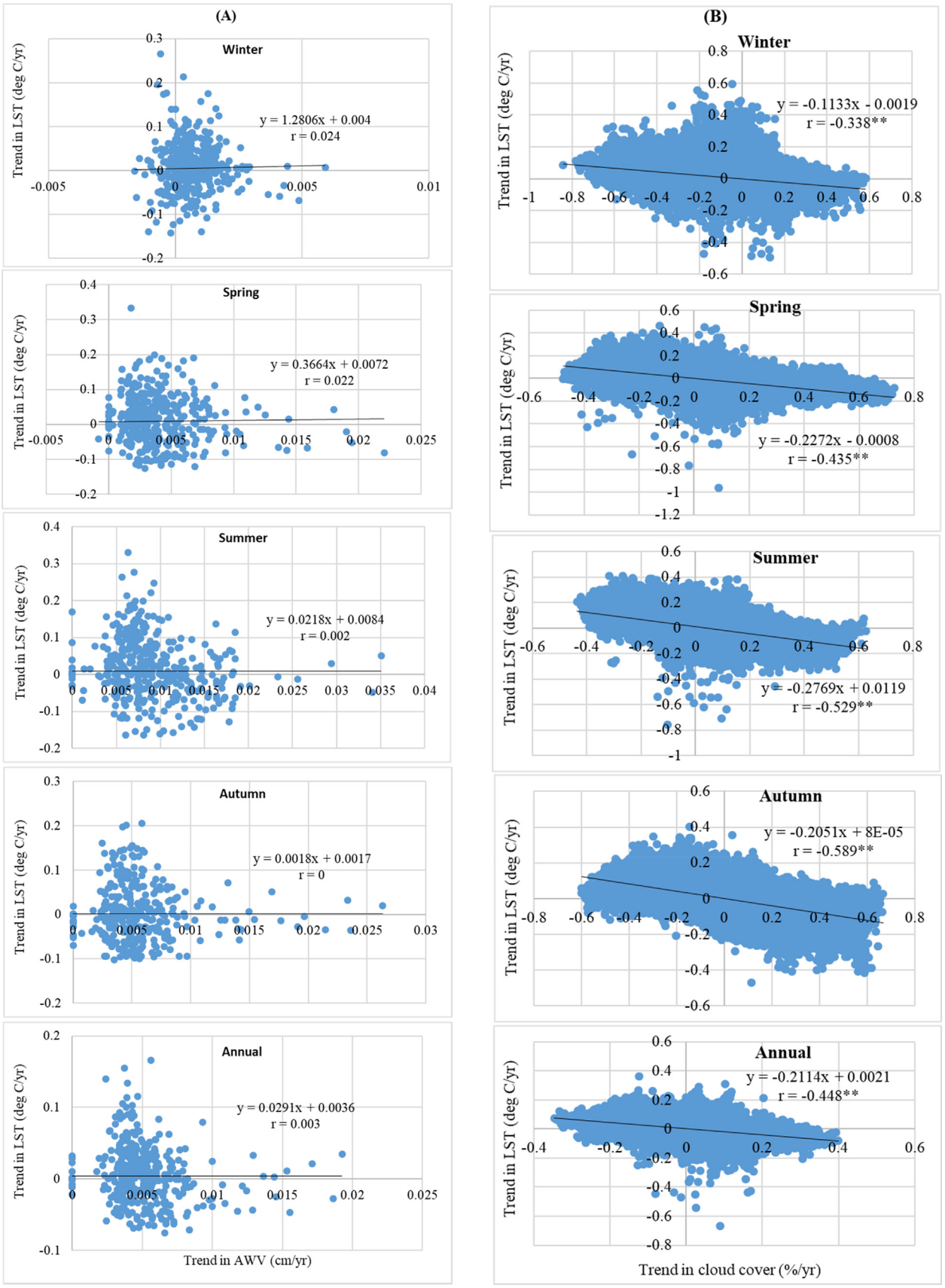

Fig. 6. Relationship of (A) LST and AWV trends and (B) LST and CF trends over the HMA during 2001–2019. (**sig at 0.01 level).

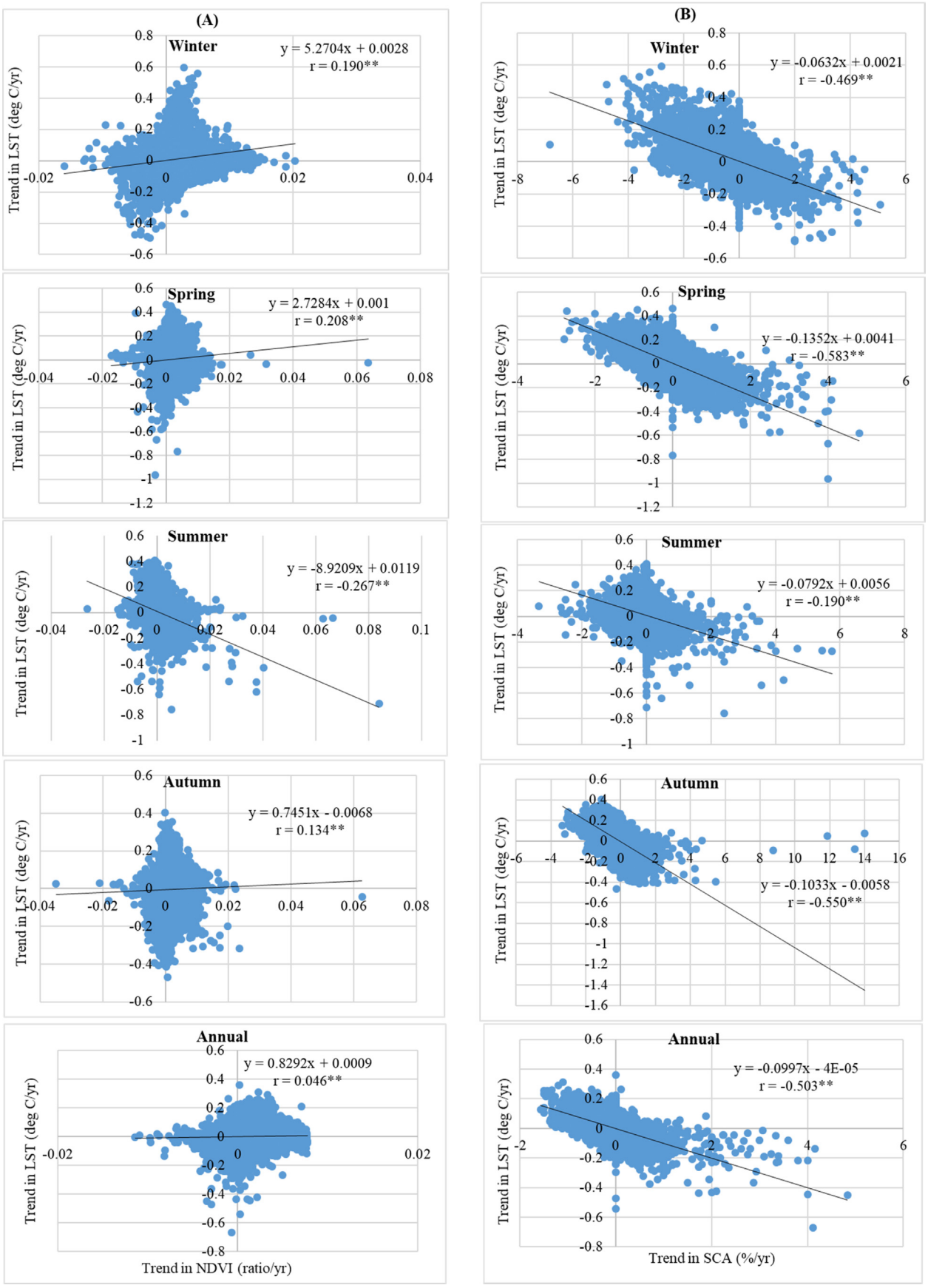

Fig. 7. Relationship of (A) LST and NDVI trends and (B) LST and SCA trends over the HMA between 2001 and 2019. (**sig at 0.01 level).

The study revealed that NDVI had a considerable influence on LST in the studied area, which is consistent with previous studies that found that NDVI effectively expresses LST in hilly terrain (Sun and Kafatos, 2007; Peng et al., 2017; Tan et al., 2020). The current study found a rising trend in NDVI in almost all the seasons (Fig. 7A), which is consistent with earlier researches (Chen et al., 2019; Zou et al., 2020). The rising NDVI values are leading to a warming trend in the vegetated areas, because of the warming effect caused by decreasing albedo in the daytime (Song et al., 2021). Albedo decreases when vegetation cover increases and variations in albedo alter the surface radiation balance, hence affecting LST.

The study found a strong negative relation of LST with SCA during the study period (Fig. 7B). SCA has high albedo that reflects a majority of the sun's energy back into the atmosphere, allowing it to regulate the flow of heat between the Earth's surface and the atmosphere, therefore having a cooling effect. The study found a significant decline of SCA in all the seasons, which is consistent with a global and regional trend (Li et al., 2018a; Li et al., 2018b; Desinayak et al., 2021). This might be one of the reasons for the region's warming in LST in the middle and high elevations (Pepin et al., 2015; Prakash and Norouzi, 2020; Sharifnezhadazizi et al., 2019), due to its positive feedback (Li et al., 2018a). During the study period (2001–2019), all four parameters had a substantial role in controlling regional LST variations in HMA, although their roles need further investigation in some mountain regions. It shows that using precise resolution remote sensing products and observed datasets in the region are needed to comprehend the role of studied drivers on LST further.

Further, the rising air temperature and decreasing precipitation in various sections of the HMA may also be the drivers of rising LST (Song et al., 2021). The precipitation in Nepal has decreased, particularly during the monsoon season (Department of Hydrology and Meteorology (DHM), 2017; Karki et al., 2017). Although long-term declining precipitation patterns are statistically insignificant, recent trends, particularly during the 1990s, are more noticeable (Shrestha et al., 2019). According to Zhao et al. (2019), in addition to the climatic warming effect, various variables such as urban expansion, changes in lowland river courses, and snow and glacier retreat have a significant impact on the local thermal environment (Bolch et al., 2019; Mal et al 2021). Furthermore, agricultural residue burning (Zhang et al., 2020) and urbanisation (Wang et al., 2021) may be contributing to the rising LST in the region. Other parameters such as slope, aspect, albedo, air temperature, precipitation, atmospheric mechanism, evapotranspiration, solar radiation, and human activities (aerosols/air pollutants, land use/land cover) must be included in future studies. A huge population lives downstream of mountain areas, which is also influenced by changes in the mountain cryosphere. Thus, the study suggests a need to further investigate the impact of all of these elements on LST to have a better knowledge of its spatial complexity and processes across the HMA.

The present study has several limitations that should be considered when interpreting the findings. The current conclusions are based on 19 years of remote sensing data, which is insufficient to assess climate change since climate change requires a longer time span (>30 years). The monthly MODIS LST data is based on clear-sky conditions only, which might reduce the data quality in some cases. To ensure the reliability of the results, future studies should employ LST data, including clear and cloudy conditions using LST reconstruction methods (e.g., diurnal temperature cycle model, random forest-based reconstruction method) (Song et al., 2021; Yang et al., 2021; Hu et al., 2020; Xiao et al., 2021). Other available longer time-series LST data can be used in a future study to fully comprehend the LST trends and their drivers. There is also the chance that MODIS daytime LST is less indicative of a few HMA regions than nighttime LST (Zhang et al., 2018b), therefore, nighttime LST trends should be considered in future studies in the HMA. Although the spatial resolution of most of the remote sensing datasets in the present study is rather good, the study encountered difficulties in a comprehensive region-elevation-wise analysis of coarser-resolution AWV and CF. It is, thus, recommended that finer resolution AWV and CF datasets be used, if available, in future studies.

6. Conclusions

The present study aims to comprehend the geographical and temporal (seasonal and annual) variations in daytime LST over the HMA from 2001 to 2019. Overall, the HMA has seen a warming trend over the years, with varying magnitudes. However, certain places are experiencing a cooling trend in LST (e.g., EHK, WH, K, CH, etc.), indicating the necessity to investigate the underlying local determinants of such a pattern. The findings of the study are as follows:

a) A considerable increase in mean daytime LST is seen over the study region at seasonal (excluding autumn) and annual scales. However, there are regional differences in mean LST trends. Among all areas, the WP had pronounced warming, while the DA experienced significant cooling. The TIM experienced enhanced warming throughout the summer, followed by the TS. The majority of the areas had a cooling trend in mean LST during the autumn. Intra-regional differences in LST across the HMA may be accounted mostly by geographical and topographical characteristics.
b) Elevation-wise, the analysis shows a clear warming trend in seasonal and annual mean LST, primarily between 4500 and 5500 m, suggesting the occurrence of EDW in the HMA. However, in certain places, EDW is not present in seasons or at annual levels (e.g. annual scale: WH, EKS, EP). It may be examined further using fine resolution datasets to corroborate these findings.
c) The spatial and temporal changes of LST in the region are influenced by AWV, CF, NDVI, and SCA. In the study region, AWV and NDVI show a positive association with LST, but CF and SCA have a negative relationship with LST. Increased LST may be caused by rising AWV, declining CF, declining SCA and rising NDVI values in the vegetated areas, but some places, in contrast, reported cooling (e.g. EHK, WH, K, CH). However, elevation in the study region controls the effects of AWV, CF, NDVI, and SCA on LST. The study suggests the necessity of exploring other additional natural and anthropogenic factors at a local level for a better understanding of its spatial complexity.

Declaration of Competing Interest

The authors declare that they have no known competing financial interests or personal relationships that could have appeared to influence the work reported in this paper.

Acknowledgments

The authors are thankful to the Earth data team for providing MODIS data in the public domain. We are also grateful to the Consultative Group for International Agricultural Research, Consortium for Spatial Information (CGIAR-CSI) for providing Shuttle Radar Topographic Mission (SRTM) data.

Appendix A. Supplementary data

Supplementary data to this article can be found online at https://doi.org/10.1016/j.ejrs.2022.04.005.

References

Avashia, V., Garg, A., Dholakia, H., 2021. Understanding temperature related health risk in context of urban land use changes. Landsc. Urban Plan. 212, 104107. https://doi.org/10.1016/j.landurbplan.2021.104107.

Bilal, H., Chamhuri, S., Mokhtar, M.B., Kanniah, K.D., 2019. Recent snow cover variation in the upper Indus basin of Gilgit Baltistan, Hindukush Karakoram Himalaya. J. Mt. Sci. 16 (2), 296–308.

Bolch, T., Kulkarni, A., Huggel, C., Paul, F., Cogley, J.G., Frey, H., Kargel, J.S., Fujita, K., Scheel, M., Bajracharya, S., Stoffel, M., 2012. The State and Fate of Himalayan Glaciers. Science 336 (6079), 310–314. https://doi.org/10.1126/science.1215828.

Bolch, T., Shea, J.M., Liu, S., Azam, F.M., Gao, Y., Gruber, S., Immerzeel, W.W., Kulkarni, A., Li, H., Tahir, A.A., Zhang, G., Zhang, Y., 2019. Status and change of the cryosphere in the Extended Hindu Kush Himalaya Region. In: Wester, P., Mishra, A., Mukherji, A., Shrestha, A.B. (Eds.), The Hindu Kush Himalaya Assessment: Mountains, Climate Change, Sustainability and People. Springer International Publishing, Cham, pp. 209–255. https://doi.org/10.1007/978-3-319-92288-1_7.

Conrad, O., Bechtel, B., Bock, M., Dietrich, H., Fischer, E., Gerlitz, L., Wehberg, J., Wichmann, V., Böhner, J., 2015. System for automated geoscientific analyses (SAGA) v. 2.1.4. Geosci. Model. Dev. 8 (7), 1991–2007.

Chen, B., Liu, Z., 2016. Global water vapor variability and trend from the latest 36 year (1979 to 2014) data of ECMWF and NCEP reanalyses, radiosonde, GPS, and microwave satellite. J. Geophys. Res. Atmos. 121 (19), 11–442.

Chen, C., Park, T., Wang, X., Piao, S., Xu, B., Chaturvedi, R.K., Fuchs, R., Brovkin, V., Ciais, P., Fensholt, R., Tømmervik, H., Bala, G., Zhu, Z., Nemani, R.R., Myneni, R.B., 2019. China and India lead in greening of the world through land-use management. Nat. Sustain 2 (2), 122–129.

Department of Hydrology and Meteorology (DHM), 2017. Observed Climate Trend Analysis of Nepal. Department of Hydrology and Meteorology, Nepal.

Desinayak, N., Prasad, A.K., El-Askary, H., Kafatos, M., Asrar, G.R., 2021. Snow cover variability and trend over Hindu Kush Himalayan region using MODIS and SRTM data. Ann. Geophys. Discuss., 1–24

Didan, K., 2015. MOD13C2 MODIS/Terra Vegetation Indices Monthly L3 Global 0.05Deg CMG V006. NASA EOSDIS Land Processes DAAC. https://doi.org/10.5067/MODIS/MOD13C2.006.

Dimri, A.P., 2021. Decoding the Karakoram Anomaly. Sci. Total Environ. 788, 147864. https://doi.org/10.1016/j.scitotenv.2021.147864.

Duan, S.-B., Li, Z.-L., Li, H., Göttsche, F.-M., Wu, H., Zhao, W., Leng, P., Zhang, X., Coll, C., 2019. Validation of Collection 6 MODIS land surface temperature product using in situ measurements. Remote Sens. Environ. 225, 16–29.

Gao, J., 2019. Global population projection grids based on Shared Socioeconomic Pathways (SSPs), downscaled 1-km grids, 2010–2100. Palisades, NY. doi.org/10.7927/H44747X4.

Earthdata Search, 2019. Greenbelt, MD: Earth Science Data and Information System (ESDIS) Project, Earth Science Projects Division (ESPD). Flight Projects Directorate, Goddard Space Flight Center (GSFC) National Aeronautics and Space Administration (NASA). https://search.earthdata.nasa.gov/.

Gao, Y., Chen, F., Lettenmaier, D.P., Xu, J., Xiao, L., Li, X., 2018. Does elevation-dependent warming hold true above 5000 m elevation? Lessons from the Tibetan Plateau. NPJ Clim. Atmos. Sci. 1 (1), 1–7.

Hall, D.K., Riggs, G.A., 2015. MODIS/Terra Snow Cover Monthly L3 Global 0.05Deg CMG, Version 6. NASA National Snow and Ice Data Center Distributed Active Archive Center, Boulder, CO.

Held, I.M., Soden, B.J., 2000. Water vapor feedback and global warming. Annu. Rev. Energy Environ 25 (1), 441–475.

Hereher, M.E., 2019. Estimation of monthly surface air temperatures from MODIS LST time series data: application to the deserts in the Sultanate of Oman. Environ. Monit. Assess. 191 (9), 1–11.

Ho, S.P., Peng, L., Mears, C., Anthes, R.A., 2018. Comparison of global observations and trends of total precipitable water derived from microwave radiometers and COSMIC radio occultation from 2006 to 2013. Atmos. Chem. Phys. 18 (1), 259–274.

Hock, R., Rasul, G., Adler, C., Cáceres, B., Gruber, S., Hirabayashi, Y., Jackson, M., Kääb, A., Kang, S., Kutuzov, S., Milner, Al., Molau, U., Morin, S., Orlove, B., Steltzer, H., 2019. High Mountain Areas. In: IPCC Special Report on the Ocean and Cryosphere in a Changing Climate. Cambridge University Press, Cambridge, UK and New York, NY, USA, pp. 131–202 https://doi.org/10.1017/9781009157964.004.

Hu, L., Sun, Y., Collins, G., Fu, P., 2020. Improved estimates of monthly land surface temperature from MODIS using a diurnal temperature cycle (DTC) model. ISPRS J. Photogramm. Remote Sens. 168, 131–140.

IPCC, 2018. Global Warming of 1.5°C. An IPCC Special Report on the impacts of global warming of 1.5°C above pre-industrial levels and related global greenhouse gas emission pathways, in the context of strengthening the global response to the threat of climate change, sustainable development, and efforts to eradicate poverty. [Masson-Delmotte, V., P. Zhai, H.-O. Pörtner, D. Roberts, J. Skea, P.R. Shukla, A. Pirani, W. Moufouma-Okia, C. Péan, R. Pidcock, S. Connors, J. B.R. Matthews, Y. Chen, X. Zhou, M.I. Gomis, E. Lonnoy, T. Maycock, M. Tignor, and T. Waterfield (eds.)]. In Press.

Jaber, S.M., Abu-Allaban, M.M., 2020. MODIS-based land surface temperature for climate variability and change research: the tale of a typical semi-arid to arid environment. Eur. J. Remote Sens. 53 (1), 81–90.

Jain, S.K., Goswami, A., Saraf, A.K., 2009. Role of elevation and aspect in snow distribution in western Himalaya. Water Resour. Manage. 23 (1), 71–83.

Jarvis, A., Reuter, H.I., Nelson, A., Guevara, E., 2008. Hole-filled SRTM for the globe version 4. Available from the CGIAR-CSI SRTM 90m Database: http://srtm.csi.cgiar.org.

Jones, B., O'Neill, B.C., 2016. Spatially explicit global population scenarios consistent with the Shared Socioeconomic Pathways. Environ. Res. Lett. 11 (8), 084003. https://doi.org/10.1088/1748-9326/11/8/084003.

Karki, R., Hasson, S., Schickhoff, U., Scholten, T., Böhner, J., 2017. Rising Precipitation Extremes across Nepal. Climate 5 (1), 1–25. https://doi.org/10.3390/cli5010004.

Kattel, D.B., Yao, T., Yang, K., Tian, L., Yang, G., Joswiak, D., 2013. Temperature lapse rate in complex mountain terrain on the southern slope of the central Himalayas. Theor. Appl. Climatol. 113 (3-4), 671–682.

Kendall, M., 1975. Rank Correlation Methods. Charles Griffin, London, U.K..

Mao, K., Yuan, Z., Zuo, Z., Xu, T., Shen, X., Gao, C., 2019. Changes in global cloud cover based on remote sensing data from 2003 to 2012. Chin. Geogr. Sci. 29 (2), 306–315.

Khandan, R., Gholamnia, M., Duan, S.B., Ghadimi, M., Alavipanah, S.K., 2018. Characterization of maximum land surface temperatures in 16 years from MODIS in Iran. Environ Res. Lett. 77, 450.

Khandelwal, S., Goyal, R., Kaul, N., Mathew, A., 2018. Assessment of land surface temperature variation due to change in elevation of area surrounding Jaipur, India. Egypt J. Remote Sens. 21 (1), 87–94.

Krishnan, R., Sanjay, J., Gnanaseelan, C., Mujumdar, M., Kulkarni, A., Chakraborty, S., 2020. Assessment of climate change over the Indian region: a report of the ministry of earth sciences (MOES), government of India (p. 226). Springer Nature.

Kuenzer, C., Dech, S., 2013. Theoretical Background of Thermal Infrared Remote Sensing. in: Kuenzer, C., Dech, S., (Eds) Thermal Infrared Remote Sensing. Remote Sensing and Digital Image Processing, vol 17. Springer, Dordrecht. https://doi.org/10.1007/978-94-007-6639-6_1.

Li, X., Wang, L., Chen, D., Yang, K., Xue, B., Sun, L., 2013. Near-surface air temperature lapse rates in the mainland China during 1962–2011. J. Geophys. Res. Atmos. 118 (14), 7505–7515.

Li, B., Chen, Y., Shi, X., 2020. Does elevation dependent warming exist in high mountain Asia? Environ. Res. Lett. 15 (2), 024012. https://doi.org/10.1088/1748-9326/ab6d7f.

Li, Q., Ma, M., Wu, X., Yang, H., 2018a. Snow cover and vegetation-induced decrease in global albedo from 2002 to 2016. J. Geophys. Res. Atmos. 123 (1), 124–138.

Li, C., Su, F., Yang, D., Tong, K., Meng, F., Kan, B., 2018b. Spatiotemporal variation of snow cover over the Tibetan Plateau based on MODIS snow product, 2001–2014. Int. J. Climatol. 38 (2), 708–728.

Li, X., Guo, W., Li, S., Zhang, J., Ni, X., 2021. The different impacts of the daytime and nighttime land surface temperatures on the alpine grassland phenology. Ecosphere 12 (6). https://doi.org/10.1002/ecs2.v12.610.1002/ecs2.3578.

Lei, Y., Letu, H., Shang, H., Shi, J., 2020. Cloud cover over the Tibetan Plateau and eastern China: a comparison of ERA5 and ERA-Interim with satellite observations. Clim. Dyn. 54 (5-6), 2941–2957.

Liu, J., Hagan, D.F.T., Liu, Y., 2021. Global land surface temperature change (2003–2017) and its relationship with climate drivers: AIRS, MODIS, and ERA5-Land based analysis. Remote Sens. 13 (1), 44.

Lu, N., Qin, J., Gao, Y., Yang, K., Trenberth, K.E., Gehne, M., Zhu, Y., 2015. Trends and variability in atmospheric precipitable water over the Tibetan Plateau for 2000–2010. Int J Climatol 35 (7), 1394–1404.

Lu, L., Zhang, T., Wang, T., Zhou, X., 2018. Evaluation of collection-6 MODIS land surface temperature product using multi-year ground measurements in an arid area of Northwest China. Remote Sens. 10 (11), 1852.

Luintel, N., Ma, W., Ma, Y., Wang, B., Subba, S., 2019. Spatial and temporal variation of daytime and nighttime MODIS land surface temperature across Nepal. Atmos. Ocean Sci. Lett. 12 (5), 305–312.

Ma, Q., You, Q., Ma, Y., Cao, Y.u., Zhang, J., Niu, M., Zhang, Y., 2021. Changes in cloud amount over the Tibetan Plateau and impacts of large-scale circulation. Atmos. Res. 249, 105332. https://doi.org/10.1016/j.atmosres.2020.105332.

Mal, S., Rani, S., Maharana, P., 2021. Estimation of spatiotemporal variability in land surface temperature over the Ganga River Basin using MODIS data. Geocarto Int. https://doi.org/10.1080/10106049.2020.1869331.

Mildrexler, D.J., Zhao, M., Cohen, W.B., Running, S.W., Song, X.P., Jones, M.O., 2018. Thermal anomalies detect critical global land surface changes. J. Appl. Meteorol. Climatol. 57 (2), 391–411.

Mildrexler, D.J., Zhao, M., Running, S.W., 2011. Satellite finds highest land skin temperatures on earth. Bull Am Meteorol Soc. 92 (7), 855–860.

Mishra, A.K., 2019. Investigating changes in cloud cover using the long-term record of precipitation extremes. Meteorol. Appl. 26 (1), 108–116.

Neeti, N., Eastman, R., 2011. A contextual Mann-Kendall approach for the assessment of trend significance in image time series. Trans. GIS 15 (5), 599–611.

Peng, W., Zhou, J., Wen, L., Xue, S., Dong, L., 2017. Land surface temperature and its impact factors in Western Sichuan Plateau, China. Geocarto Int. 32 (8), 919–934.

Peng, X., Wu, W., Zheng, Y., Sun, J., Hu, T., Wang, P., 2020. Correlation analysis of land surface temperature and topographic elements in Hangzhou, China. Sci. Rep. 10 (1), 1–16.

Pepin, N., Bradley, R.S., Diaz, H.F., Baraer, M., Caceres, E.B., Forsythe, N., Fowler, H., Greenwood, G., Hashmi, M.Z., Liu, X.D., et al., 2015. Elevation-dependent warming in mountain regions of the world. Nat. Clim. Change. 5, 424–430.

Pepin, N., Deng, H., Zhang, H., Zhang, F., Kang, S., Yao, T., 2019. An examination of temperature trends at high elevations across the Tibetan Plateau: the use of MODIS LST to understand patterns of elevation dependent warming. J. Geophys. Res. Atmos. 124 (11), 5738–5756.

Platnick, S., Hubanks, P., Meyer, K., King, M.D., 2015. MODIS Atmosphere L3 Monthly Product (08_L3). NASA MODIS Adaptive Processing System, Goddard Space Flight Center. https://doi.org/10.5067/MODIS/MOD08_M3.006 (Terra).

Prakash, S., Norouzi, H., 2020. Land surface temperature variability across India: a remote sensing satellite perspective. Theor. Appl. Climatol. 139 (1-2), 773–784.

Prakash, S., Shati, F., Norouzi, H., Blake, R., 2019. Observed differences between near-surface air and skin temperatures using satellite and ground-based data. Theor. Appl. Climatol. 137 (1–2), 587–600.

Qin, J., Yang, K., Liang, S., Guo, X., 2009. The altitudinal dependence of recent rapid warming over the Tibetan Plateau. Clim. Change. 97 (1–2), 321–327.

Riggs, G.A., Hall, D.K., Roman, M.O., 2019. MODIS snow products collection 6.1 user guide version 1.0. Greenbelt, MD: NASA Goddard Space Flight Center.

Rao, Y., Liang, S., Wang, D., Yu, Y., Song, Z., Zhou, Y., Shen, M., Xu, B., 2019. Estimating daily average surface air temperature using satellite land surface temperature and top-of-atmosphere radiation products over the Tibetan Plateau. Remote Sensing of Environment 234 (1), 1–14. https://doi.org/10.1016/j.rse.2019.111462.

Romshoo, S.A., Rafiq, M., Rashid, I., 2018. Spatio-temporal variation of land surface temperature and temperature lapse rate over mountainous Kashmir Himalaya. J. Mt. Sci. 15 (3), 563–576.

Sen, P., 1968. Estimates of the regression coefficient based on Kendall's tau. J. Am. Stat. Assoc. 63 (324), 1379–1389.

Shafiq, M.U., Ahmed, P., Islam, Z.U., Joshi, P.K., Bhat, W.A., 2019. Snow cover area change and its relations with climatic variability in Kashmir Himalayas, India. Geocarto Int 34 (6), 688–702.

Sharifnezhadazizi, Z., Norouzi, H., Prakash, S., Beale, C., Vardi, R., 2019. A global analysis of land surface temperature diurnal cycle using modis observations. J. Appl. Meteorol. Climatol. 58 (6), 1279–1291.

Shrestha, S., Yao, T., Adhikari, T.R., 2019. Analysis of rainfall trends of two complex mountain river basins on the southern slopes of the Central Himalayas. Atmos. Res. 215, 99–115.

Singh, R.P., Paramanik, S., Bhattacharya, B.K., Behera, M.D., 2020. Modelling of evapotranspiration using land surface energy balance and thermal infrared remote sensing. Trop. Ecol., 1–9

Song, Z., Li, R., Qiu, R., Liu, S., Tan, C., Li, Q., Ge, W., Han, X., Tang, X., Shi, W., Song, L., 2018. Global land surface temperature influenced by vegetation cover and PM2.5 from 2001 to 2016. Remote Sens. 10 (12), 2034.

Song, Z., Yang, H., Huang, X., Yu, W., Huang, J., Ma, M., 2021. The spatiotemporal pattern and influencing factors of land surface temperature change in China from 2003 to 2019. Int. J. Appl. Earth Obs. Geoinf. 104, 102537.

Sun, D., Kafatos, M., 2007. Note on the NDVI-LST relationship and the use of temperature-related drought indices over North America. Geophys. Res. Lett. 34 (24), 1–4.

Sun, Z., Wan, H., Imbery, S., Lotz, T., King, L., 2015. Dynamics of land surface temperature in the Central Tien Shan Mountains. Mt. Res. Dev. 35 (4), 328–337.

Tan, J., Yu, D., Li, Q., Tan, X., Zhou, W., 2020. Spatial relationship between land-use/land-cover change and land surface temperature in the Dongting Lake area, China. Sci. Rep. 10 (1), 1–9.

Theil, H., 1950. A rank-invariant method of linear and polynomial regression analysis. Koninkluke Nederlandse Akademie Van Wet.enschappen. 53, 467–482.

Thiebault, K., Young, S., 2020. Snow cover change and its relationship with land surface temperature and vegetation in northeastern North America from 2000 to 2017. Int. J. Remote Sens. 41 (21), 8453–8474.

Wang, R., Liu, Y., 2020. Recent declines in global water vapor from MODIS products: Artifact or real trend? Remote Sens. Environ. 247, 111896.

Wang, J., Dai, A., Mears, C., 2016. Global water vapor trend from 1988 to 2011 and its diurnal asymmetry based on GPS, radiosonde, and microwave satellite measurements. J. Clim. 29 (14), 5205–5222.

Wang, Y., Yi, G., Zhou, X., Zhang, T., Bie, X., Li, J., Ji, B., 2021. Spatial distribution and influencing factors on urban land surface temperature of twelve megacities in China from 2000 to 2017. Ecol. Indic. 125, 107533.

World Meteorological Organization (WMO) 2020a State of the Global Climate 2020 (WMO-No. 1264) https://library.wmo.int/doc_num.php?explnum_id=10618.

World Meteorological Organization (WMO) 2020b State of the Climate in Asia 2020 (WMO-No. 1273) https://library.wmo.int/doc_num.php?explnum_id=10867.

Wan, Z., 2015. MYD11C3 MODIS/aqua land surface temperature and the emissivity monthly l3 global 0.05 deg CMG. University of California Santa Barbara, Simon Hook, Glynn Hulley - JPL and MODAPS SIPS - NASA. NASA LP DAAC. http://doi.org/10.5067/MODIS/MYD11C3.006.

Wan, Z., 2013 Collection-6 MODIS Land Surface Temperature Products Users' Guide. https://lpdaac.usgs.gov/documents/118/MOD11_User_Guide_V6.pdf.

Yang, M., Zhao, W., Zhan, Q., Xiong, D., 2021. Spatiotemporal patterns of land surface temperature change in the Tibetan plateau based on MODIS/Terra daily product from 2000 to 2018. IEEE J. Sel. Top. Appl. Earth Obs. Remote Sens. 14, 6501–6514.

Yue, J., Russell III, J., Gan, Q., Wang, T., Rong, P., Garcia, R., Mlynczak, M., 2019. Increasing water vapor in the stratosphere and mesosphere after 2002. Geophys. Res. Lett. 46 (22), 13452–13460.

Xiao, Y., Zhao, W., Ma, M., He, K., 2021. Gap-free LST generation for MODIS/Terra LST product using a random forest-based reconstruction method. Remote Sens. 13 (14), 2828.

Zou, F., Li, H., Hu, Q., 2020. Responses of vegetation greening and land surface temperature variations to global warming on the Qinghai-Tibetan Plateau, 2001–2016. Ecol. Indic 119, 106867.

Zafar, M.U., Ahmed, M., Rao, M.P., Buckley, B.M., Khan, N., Wahab, M., Palmer, J., 2016. Karakorum temperature out of phase with hemispheric trends for the past five centuries. Clim. Dyn. 46 (5–6), 943–1952.

Zhang, Y., Xu, J., Yang, N., Lan, P., 2018a. Variability and trends in global precipitable water vapor retrieved from COSMIC radio occultation and radiosonde observations. Atmosphere 9 (5), 174.

Zhang, H., Zhang, F., Zhang, G., Che, T., Yan, W., 2018b. How accurately can the air temperature lapse rate over the Tibetan Plateau be estimated from MODIS LSTs? J. Geophys. Res. Atmos. J 123 (8), 3943–3960.

Zhang, W., Yu, M., He, Q., Wang, T., Lin, L., Cao, K., Huang, W., Fu, P., Chen, J., 2020. The spatial and temporal impact of agricultural crop residual burning on local land surface temperature in three provinces across China from 2015 to 2017. J. Clean. Prod. 275, 124057.

Zhao, W., He, J., Wu, Y., Xiong, D., Wen, F., Li, A., 2019. An analysis of land surface temperature trends in the central Himalayan region based on MODIS products. Remote Sens. 11 (8), 1–19.

Zhao, W., Xiong, D., Wen, F., Wang, X., 2020a. Lake area monitoring based on land surface temperature in the Tibetan Plateau from 2000 to 2018. Environ. Res. Lett. 15, (8) 084033.

Zhao, B., Mao, K., Cai, Y., Shi, J., Li, Z., Qin, Z., Meng, X., Shen, X., Guo, Z., 2020b. A combined Terra and Aqua MODIS land surface temperature and meteorological station data product for China from 2003 to 2017. Earth Syst. Sci. Data 12 (4), 2555–2577.